Check for updates

The Tyrosine Phosphatase PRL Regulates Attachment of *Toxoplasma gondii* to Host Cells and Is Essential for Virulence

Chunlin Yang,[a] William J. Blakely,[a] Gustavo Arrizabalaga[a,b]

[a]Department of Pharmacology and Toxicology, Indiana University School of Medicine, Indianapolis, Indiana, USA
[b]Department of Microbiology and Immunology, Indiana University School of Medicine, Indianapolis, Indiana, USA

ABSTRACT The pathogenesis of *Toxoplasma gondii* is mainly due to tissue damage caused by the repeating lytic cycles of the parasite. Many proteins localized to the pellicle of the parasite, particularly kinases, have been identified as critical regulators of the *Toxoplasma* lytic cycle. However, little is known about the associated protein phosphatases. Phosphatase of regenerating liver (PRL), a highly conserved tyrosine phosphatase, is an oncoprotein that plays pivotal roles in mammalian cells and typically associates with membranes via a conserved prenylation site. PRL in *Toxoplasma* has a predicted prenylation motif in the C terminus, like other homologs. We have determined that *T. gondii* PRL (TgPRL) localizes to the plasma membrane and that disruption of TgPRL results in a defect in the parasite's ability to attach to host cells. This function is dependent on both TgPRL's membrane localization and phosphatase activity. Importantly, *in vivo* experiments have shown that while mice infected with parental strain parasites die within days of infection, those infected with parasites lacking TgPRL not only survive but also develop immunity that confers protection against subsequent infection with wild-type parasites. Immunoprecipitation experiments revealed that the PRL-CNNM (cyclin M) complex, which regulates intracellular Mg^{2+} homeostasis in mammalian cells, is also present in *Toxoplasma*. Consistent with this interaction, parasites lacking TgPRL had higher intracellular Mg^{2+} levels than the parental or complemented strains, suggesting TgPRL is involved in regulating intracellular Mg^{2+} homeostasis. Thus, TgPRL is a vital regulator of the *Toxoplasma* lytic cycle and virulence, showing its potential as a target of therapeutic intervention.

IMPORTANCE Infection with *Toxoplasma gondii* can lead to severe and even life-threatening diseases in people with compromised or suppressed immune systems. Unfortunately, drugs to combat the parasite are limited, highly toxic, and ineffective against the chronic stage of the parasite. Consequently, there is a strong demand for the discovery of new treatments. A comprehensive understanding of how the parasite propagates in the host cells and which proteins contribute to the parasite's virulence will facilitate the discovery of new drug targets. Our study meets this objective and adds new insights to understanding the lytic cycle regulation and virulence of *Toxoplasma* by determining that the protein phosphatase TgPRL plays a vital role in the parasite's ability to attach to host cells and that it is essential for parasite virulence.

KEYWORDS PRL, *Toxoplasma*, tyrosine phosphatase, virulence, attachment, magnesium, parasite

Toxoplasma gondii is a single-celled parasite of the phylum Apicomplexa, capable of infecting any warm-blooded animal, including approximately 30% of humans worldwide (1, 2). Humans are infected congenitally or by ingestion of either environmental oocysts, shed in the feces of cats, or tissue cysts in undercooked meat of infected animals. Most infections are asymptomatic during the acute stage, but to

evade the immune response, the parasite converts to a latent encysted form, thus establishing a chronic infection (3). In immunocompromised individuals, such as lymphoma and AIDS patients, new infections or reactivation of parasites in preexisting cysts can lead to severe toxoplasmic encephalitis (4). In addition, for congenital infections, given the immature nature of the fetal immune system, toxoplasmosis can lead to blindness, severe neurological problems, and even death (5, 6).

A significant portion of the pathogenesis associated with toxoplasmosis is a direct consequence of the repeating cycles of invasion, division, and egress that drive the propagation of the parasite (7, 8). Both invasion and egress of the parasite are active events that rely on regulated secretion from specialized organelles and on the parasite's gliding motility system (9, 10). Secretion and motility are tightly regulated by opposing effects of cGMP and cAMP and by calcium signaling (11–14). Particularly, calcium-dependent phosphorylation plays a key role in the regulation of the parasite's lytic cycle (15–18). While many of the kinases involved in regulating the effectors of the lytic cycle have been elucidated (19–21), little is known about the role of phosphatases. Strong candidate phosphatases for roles in lytic cycle regulation are those that associate with the parasite's pellicle and cytoskeleton as they are critical for both motility and secretion. Recently, we characterized serine/threonine protein phosphatases predicted to be membrane associated and determined that only PPM5C, a PP2C family protein phosphatase, localizes to the plasma membrane, where it regulates attachment of *Toxoplasma* to host cells (22).

One member of the tyrosine protein phosphatases of *Toxoplasma* that may also be associated with the pellicle is a homolog of the phosphatase of regenerating liver (PRL). PRL is a highly conserved tyrosine phosphatase that possesses a prenylation motif at the C terminus (23). Typically, prenylation and the polybasic region preceding it guide PRL homologs to the plasma membrane (23). PRL was first identified in regenerating livers because of its highly elevated expression (24)—hence its name. Mammalian cells encode three PRLs, which show significant amino acid sequence identity. N-terminal epitope-tagged mouse PRLs were shown to be present in the inner leaflet of the plasma membrane and in intracellular punctate structures that were determined to be early endosomes (25). However, studies using antibodies against mammalian PRLs have identified variable localizations. For instance, PRL1 was found to be present in the endoplasmic reticulum and mitotic spindle (26), and PRL3 and PRL1 were found in the plasma membrane and cytoplasm (27). Multiple studies have indicated that PRL genes are oncogenic and are overexpressed in a wide variety of cancer cells, especially in metastatic lesions (28–30). As their expression levels in cancer cells closely correlate with disease progression, PRLs are considered potential therapeutic targets for cancer treatment (31). Although PRLs play vital roles in the regulation of cancer progression, the molecular mechanisms behind their function remain unclear (23, 31). Studies have shown PRL is involved in a breadth of cell signaling pathways, including Rho family GTPase, phosphatidylinositol 3-kinase (PI3K)-Akt, Ras–mitogen-activated protein kinase (MAPK), STATs, P53, and Src/extracellular signal-regulated kinase 1/2 (ERK1/2) (23, 31). However, no clear substrates of PRL in these signaling pathways have been identified so far.

Despite the important role of PRL in mammalian cells, its function in apicomplexan parasites is poorly understood. The *Plasmodium falciparum* homolog PfPRL is 218 amino acids in length and contains the conserved C-terminal signature CAAX motif CHFM for prenylation. *In vitro* phosphatase activity assays indicated that PfPRL is a tyrosine phosphatase, as it is preferentially inhibited by a tyrosine phosphatase inhibitor (32). An immunofluorescence assay (IFA) using antibodies against PfPRL showed that PfPRL is present in the endoplasmic reticulum and a subcompartment of the food vacuole when the parasite is in intraerythrocytic stages (32). In contrast, the *T. gondii* homolog (TgPRL) has not been characterized. TgPRL is slightly larger than the human and *Plasmodium* homologs, with 404 residues, and has a C-terminal prenylation motif, CAIM. In this study, we determined that the TgPRL associates with the parasite membrane and that it regulates attachment to host cells. Importantly, deletion of *TgPRL*
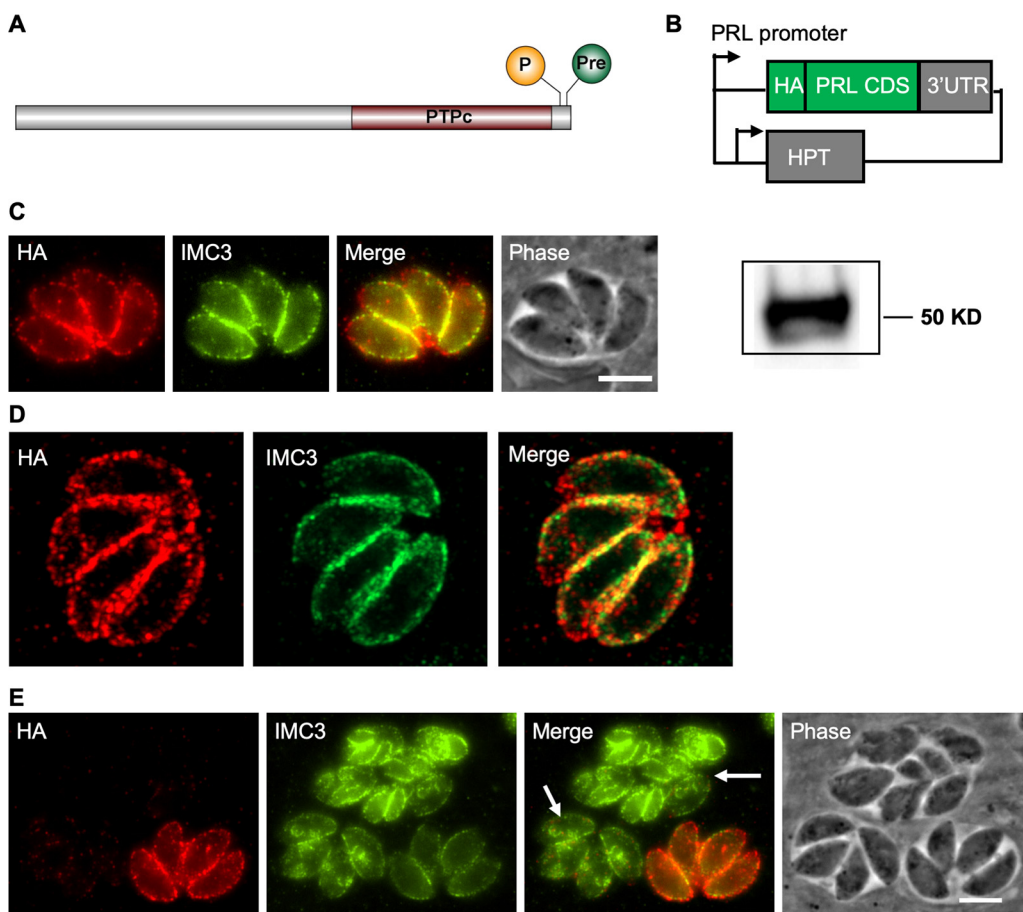
FIG 1 TgPRL localizes to the plasma membrane. (A) Schematic of TgPRL showing the palmitoylation (P) and prenylation (Pre) sites and the tyrosine phosphatase domain (PTPc); (B) diagram of the HA-PRL expression plasmid. One copy of an HA epitope tag is included at the N terminus of the TgPRL coding sequences. Expression of the fused HA-PRL is under the control of the *TgPRL* promoter. The plasmid also contains the selectable marker HXGPRT (HPT). (C) Intracellular parasites expressing HA-PRL were stained with antibodies against the HA epitope (red) and IMC3 (green). Scale bar = 2 μm. The panel to the right of panel C shows the Western blot of parasite extracts probed for HA. (D) The same IFA sample of panel C was observed with a laser confocal microscope. (E) Panels show both dividing (arrow) and not dividing HA-PRL-expressing parasites stained as in panel C.

renders the parasite avirulent, which reveals the potential of this protein as a target for therapeutic intervention.

RESULTS

TgPRL is localized to the plasma membrane. Like its homologs in human cells, TgPRL has a C-terminal prenylation motif, indicating that it is likely membrane associated (Fig. 1A). In addition, a predicted palmitoylation site of four amino acids upstream of the prenylation motif increases the likelihood of its localization in the plasma membrane (Fig. 1A). To determine the localization of TgPRL, we constructed an ectopic expression plasmid that uses TgPRL's promoter to drive expression of TgPRL carrying a hemagglutinin (HA) epitope tag at the N terminus (Fig. 1B). A parasite strain stably carrying this construct (Δ*hx*::HA-PRL) was established, and expression of HA-tagged TgPRL at the expected size (45.08 kDa) was confirmed by Western blot (Fig. 1C). An immunofluorescence assay (IFA) of the resulting strain showed that the N-terminal HA-tagged TgPRL mainly localizes to the plasma membrane, as expected, with some punctate staining in the cytoplasm (Fig. 1C and D). Due to the lack of any secretory signal peptide, TgPRL is expected to be localized to the inner side of the plasma membrane facing the cytoplasm, like its mammalian homologs. Interestingly, the N-terminal HA-tagged TgPRL appears to be normally
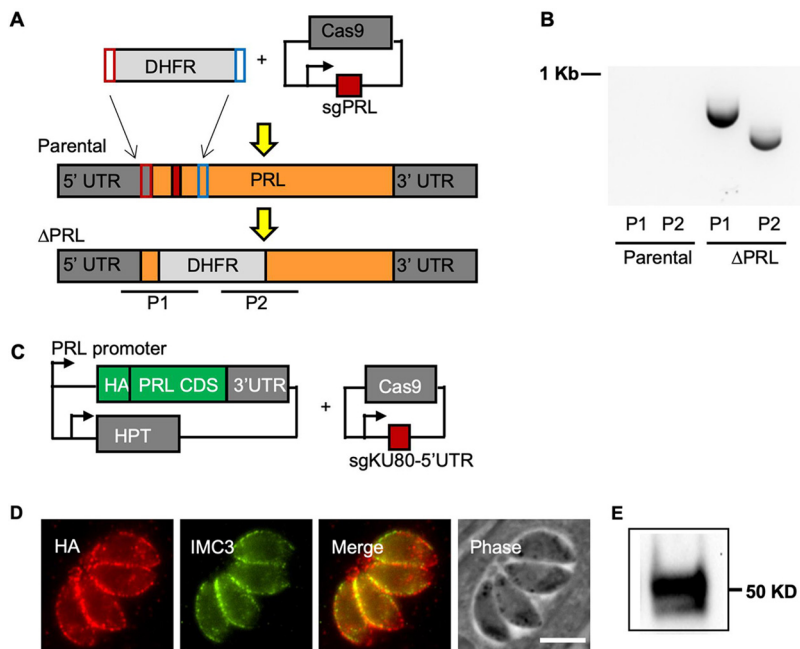
FIG 2 Generation and complementation of the TgPRL knockout strain. (A) The diagram depicts the strategy used for developing the TgPRL knockout Δ*prl* strain. Parasites were transfected with a plasmid encoding Cas9 and a guide RNA that targets the first exon of *TgPRL* (red box) as well as an amplicon that contains the selectable marker DHFR and regions of homology to the *TgPRL* locus. The bottom graphic represents the resulting edited genome in the knockout strain. P1 and P2 are the regions amplified by PCR to confirm disruption. (B) Results of PCR of both parental and Δ*prl* strains for amplicons P1 and P2 are shown. (C) A diagram depicts the plasmids used to develop the TgPRL complementation (Δ*prl*.cp) strain. The HA-PRL expression plasmid is the same one shown in Fig. 1B. A plasmid that expresses Cas9 and a guide RNA targeting the 5′ UTR of the KU80 gene was used to locate the expression cassette. (D, E) Expression of HA-PRL in the complemented strain was confirmed by immunofluorescence assays (D) and Western blot (E).

expressed in nondividing parasites but is poorly expressed in parasites with developing daughter parasites (Fig. 1E).

Knockout of TgPRL affects *Toxoplasma* propagation. To determine the function of TgPRL in *Toxoplasma*, we generated a knockout (KO) strain of TgPRL using a CRISPR/Cas9-driven approach (Fig. 2A) (33). Briefly, we constructed a plasmid, pSag1-Cas9-U6-sgPRL, which expresses Cas9 and a guide RNA targeting the first exon of the *TgPRL* gene, and generated a PCR amplicon containing a selectable dihydrofolate reductase (DHFR) marker (34) flanked by overhangs with homology to *TgPRL* sequences upstream and downstream of the Cas9 cut site (Fig. 2A). Both the plasmid and the amplicon were transfected into parasites lacking KU80 (Δ*ku80*) (35) to favor homologous recombination (Fig. 2A). PCR with primers flanking the cut site was performed, and the resulting amplicons were sequenced to validate the successful insertion of the selection marker (Fig. 2B). To attribute any defect observed in the Δ*prl* parasite strain, we introduced an N-terminal HA-tagged TgPRL at the 5′ untranslated region (5′ UTR) of the disrupted *KU80* gene for complementation (Fig. 2C). The resulting complemented (Δ*prl*.cp) strain was confirmed for the expression of HA-PRL by both Western blotting and IFA (Fig. 2D and E).

To examine the effect of disrupting TgPRL on parasite propagation, we performed plaque assays of the parental (Δ*ku80*), knockout (Δ*prl*), and complemented (Δ*prl*.cp) strains. This assay showed that Δ*prl* parasites formed significantly smaller plaques than the parental strain, indicating that disruption of TgPRL affects parasite propagation (Fig. 3A and B). On average, the knockout strain cleared 47.8% ± 7.6% of the cell monolayer relative to the parental strain, while the complemented strain cleared 72.5% ± 5.7%. This piece of data is consistent with the predicted fitness score (−2.32)
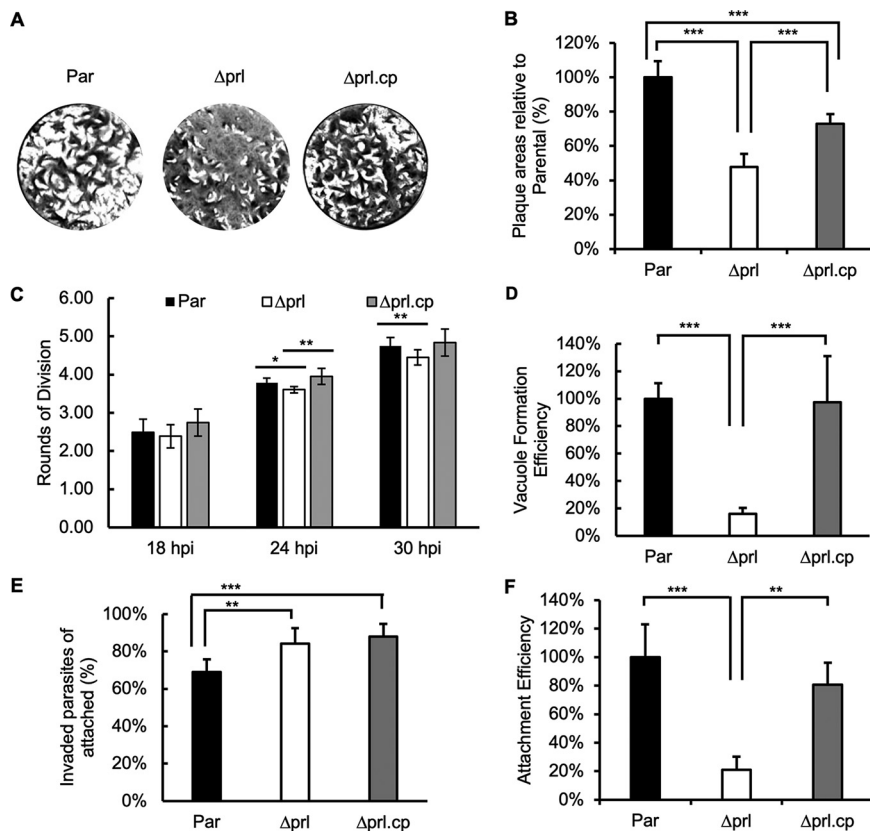
FIG 3 Phenotypic analysis of the TgPRL knockout strain. Assays were performed to determine the ability of the knockout (Δ*prl*) strain in propagation, replication, invasion, and attachment of parasites with comparison to the parental (Par) and complemented (Δ*prl*.cp) strains. (A) Representative images of plaque assays are shown. (B) The graph represents the quantification of area cleared by plaques relative to the parental strain for all strains. (C) For each strain, we quantified the average number of rounds of division at 18, 24, and 30 h postinfection (hpi). (D) Parasites of each strain were allowed to invade cells for 30 min, and the number of vacuoles formed was quantitated. Data are shown as a percentage of efficiency in relation to the parental strain. (E) Parasites were allowed to invade for 30 min, and parasites that were attached but not invaded and those that were invaded were differentially stained to quantitate invasion. The bars represent the percentage of invaded parasites in the 10 randomly selected fields of view. (F) Results from the same experiment as panel E were analyzed to quantitate attachment efficiency across all three strains. The bars represent the total number of parasites, including both those attached and invaded in the 10 randomly selected fields of view. The data presented are normalized to the average of the data obtained from parental parasites. For all data graphs, $n = 3$ biological replicates $\times$ 3 experimental replicates, and the P value was estimated by two-tailed Student's t test. Error bars show standard deviations (SD). *, $P < 0.01$; **, $P < 0.001$; ***, $P < 0.0001$.

of TgPRL obtained from a genome-wide CRISPR screen (36). Importantly, the expression of an N-terminal HA-tagged TgPRL in the knockout strain was able to partially complement the phenotype, confirming the link between the knockout of TgPRL and the phenotype (Fig. 3A and B). As the expression of TgPRL is tightly regulated during the division cycle, it is possible that the lack of full complementation is due to the exogenous copy of TgPRL not fully recapitulating the expression level and pattern of the endogenous protein.

Knockout of TgPRL causes a defect in host cell attachment. Reduction in plaque size can be due to a disruption in any of the multiple steps that make up the *Toxoplasma* propagation cycle, including attachment, invasion, division, egress, and motility (8). Accordingly, we performed a series of more precise phenotypic assays to identify the specific step affected by *TgPRL* genetic disruption. To compare the division rates of the different strains, we allowed parasites to infect host cells for 30 min, after which cultures were incubated for 18, 24, or 30 h before fixation. For each data point, we scored the number of parasites per vacuole for at least 50 vacuoles and

converted the average parasite per vacuole value to the corresponding rounds of cell divisions (Fig. 3C). This assay showed that the Δ*prl* parasites are slightly behind division rounds at 24 h (parental, 3.78, versus Δ*prl*, 3.60) and 30 h (parental, 4.75, versus Δ*prl*, 4.45) postinfection (Fig. 3C). While small, these differences are statistically significant and were complemented by reintroducing the wild-type (WT) copy of the gene.

Next, we analyzed the ability of Δ*prl* parasites to enter host cells and establish parasitophorous vacuoles compared to those of the parental and complemented strains. We found that the percentage of vacuoles formed by Δ*prl* parasites was 15.9% ± 4.5%, while the complemented strain formed 97.3% ± 33.8% of vacuoles relative to the parental strain (Fig. 3D). These results suggest that the propagation phenotype observed with the Δ*prl* parasites is likely due to the defect in parasite entry into host cells.

The mutant parasite's reduced ability to form vacuoles could be due to inefficient attachment, invasion, or both. Accordingly, we performed an invasion assay, in which the outside noninvaded but stably attached parasites were stained green with antibody against the cell surface antigen Sag1 before permeabilization of the cell membrane, and all parasites (both inside and outside) were stained red with anti-Mic5 antibody after membrane permeabilization (37). In this way, we can compare the efficiency of attachment and invasion between strains. Attachment efficiency is assessed based on the total number of parasites detected, both inside and outside the cell, since those that have invaded must have attached first. Meanwhile, invasion efficiency is assessed based on the percentage of parasites that are inside the cell (i.e., inside/total). When comparing the percentages of total parasites that are inside cells, we noted that Δ*prl* and complemented parasite strains have a slightly higher invasion efficiency (Fig. 3E). In contrast, we noted a significant difference across strains when we quantitated the total number of parasites detected both outside and inside cells, indicating a difference in attachment efficiency. The total number of attached Δ*prl* parasites was 21.0% ± 9.1% relative to the parental strain, while that of the complemented strain was 80.7% ± 15.2% relative to the parental strain, again showing partial complementation of the phenotype (Fig. 3F). This assay indicates that disruption of TgPRL severely impairs the parasite's ability to attach to host cells.

The establishment of a tight attachment of the parasites to host cells is mediated by several adhesion proteins secreted from micronemes in a calcium-dependent manner (38, 39). To determine whether the defect in the attachment of the Δ*prl* parasites is the result of deficient microneme secretion, we monitored secretion of the microneme marker MIC2 across the parental, mutant, and complemented strains. We detected no difference in the levels of constitutive secretion of MIC2 among the three strains (see Fig. S1 in the supplemental material). In addition, we also detected no difference in the amounts of calcium-induced secretion of MIC2 among the three strains (Fig. S1). Moreover, there was also no significant difference in secretion from the dense granules, another set of secretory organelles, determined by monitoring Gra1 (Fig. S1). Taken together, these data suggest that the role of TgPRL in attachment is likely independent of microneme secretion.

Localization and activity are important for TgPRL's role in attachment. To explore whether the localization of TgPRL in the plasma membrane is necessary for its role in host cell attachment, we mutated the HA-PRL expression plasmid so that the conserved cysteine predicted to be prenylated was mutated to alanine (C401A). The C401A plasmid was transfected into the Δ*prl* parasites using the same approach as for the complementation with the wild-type TgPRL described above. IFA of the established parasite strain showed that the C401A mutant TgPRL was distributed throughout the cytoplasm, and no detectable association with the plasma membrane was observed (Fig. 4A), suggesting the prenylation site of TgPRL is required for its localization. Importantly, the mislocalized C401A mutant TgPRL was unable to complement the plaque-forming phenotype of Δ*prl* parasites (Fig. 4B). This indicates that membrane association is critical for TgPRL's function in the lytic cycle.

Typically, a cysteine at the center of tyrosine phosphatase domains is required for establishing a phosphoryl-cysteine intermediate (PTP-Cys-PO_3) and thus phosphatase
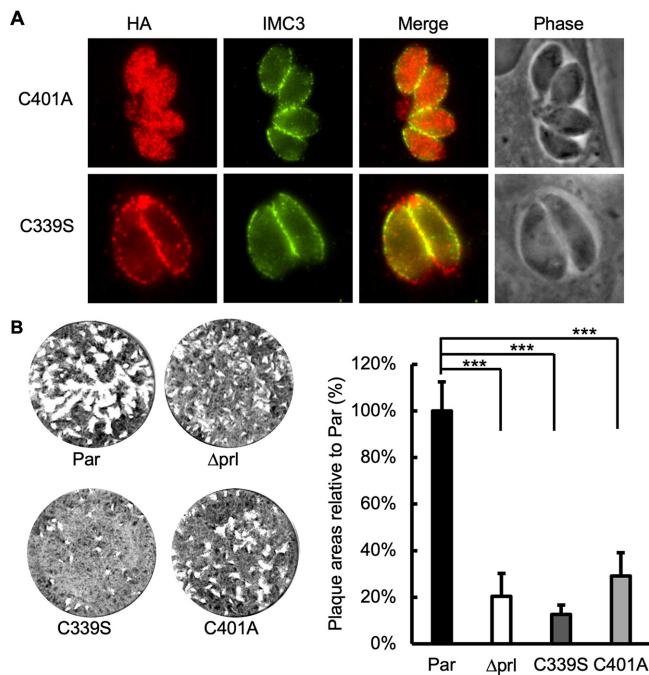
FIG 4 Role of membrane localization and phosphatase activity in TgPRL function. The Δ*prl* knockout strain was transfected with mutant versions (C339S and C401A) of the complementation plasmid shown in Fig. 2C. (A) Intracellular parasites expressing the C339S or C401A mutant TgPRL were stained to determine the localization of exogenous mutant TgPRL. As expected, the C339S mutant correctly associates with the plasma membrane, and the C401A mutant is mislocalized to the cytoplasm of the parasite. (B) Representative images of the plaque assay of corresponding strains. The chart on the right is the quantification of the plaque area relative to the parental strain. For all data, $n = 3$ biological replicates × 3 experimental replicates, and the P value was estimated by two-tailed Student's t test. Error bars show standard deviations. ***, $P < 0.0001$.

function (40). Accordingly, to determine if the phosphatase activity is important for TgPRL's role in attachment, we mutated the conserved cysteine in the center of the phosphatase domain into serine (C339S) in the HA-PRL expression plasmid and transfected it into the Δ*prl* parasites for complementation. The IFA of the resulting strain showed that the C339S mutant TgPRL localized correctly to the plasma membrane (Fig. 4A). Nonetheless, the plaque assays showed that the C339S mutant formed only 12.7% ± 3.9% of plaques relative to the parental strain, while the Δ*prl* parasites formed 20.4% ± 9.9%, indicating that the C339S mutant TgPRL not only failed to rescue the phenotype but further decreased the plaque-forming deficiency of the mutant strain (Fig. 4B). In conjunction, these results indicate that TgPRL phosphatase activity at the periphery of the parasite is required for the protein's function during host cell attachment.

Identification of TgPRL's potential substrates and interactors. To identify potential substrates and interactors of TgPRL, we performed a coimmunoprecipitation (co-IP) assay with an HA-PRL-expressing strain. Since the interaction between phosphatases and their substrates can be transient and unstable, we used cross-linking with disuccinimidyl sulfoxide (DSSO) prior to immunoprecipitation to stabilize protein-protein interactions. Co-IP was performed by using mouse anti-HA magnetic beads to capture HA-PRL and interacting proteins in the lysate of Δ*prl*.cp parasites, with the parental Δ*ku80* parasites as a control. The proteins pulled down by the beads were identified by using mass spectrometry (MS). The obtained data (Data Set S1) were curated with the following criteria to develop a list of putative TgPRL substrates or interactors: no less than five peptides and fold change of peptides over the control of ≥8. Applying these criteria resulted in a list of 18 putative TgPRL interactors (Table 1).

Interestingly, one of the most abundant prey proteins in the list is a cystathionine-β-synthase (CBS) domain-containing protein (TGGT1_211350), which contains an

TABLE 1 Putative TgPRL-interacting protein partners and substrates identified by coimmunoprecipitation and mass spectrometry

ID (ToxoDB.org)	Function Annotation	No. of peptides	
		Control ($\Delta ku80$)	Δprl.cp
TGGT1_208718	Putative protein tyrosine phosphatase type IVA A (PRL)	0	54
TGGT1_287980	FHA domain-containing protein	0	17
TGGT1_202840	FHA domain-containing protein	0	12
TGGT1_262150	Kelch repeat and K^+ channel tetramerization domain-containing protein	0	11
TGGT1_278660	Putative P-type ATPase 4	0	9
TGGT1_211350	CBS domain-containing protein (CNNM1)	0	8
TGGT1_297520	Proteophosphoglycan PPG1	0	8
TGGT1_219700	Putative DNA replication licensing factor MCM4	0	6
TGGT1_227800	EF-hand domain-containing protein	0	6
TGGT1_243920	Putative DNA replication licensing factor MCM5	0	6
TGGT1_263130	Putative citrate synthase	0	6
TGGT1_289970	Hypothetical protein	0	5
TGGT1_311830	Hypothetical protein	0	5
TGGT1_314400	Putative pyruvate dehydrogenase E1 component, beta subunit	1	10
TGGT1_219860	Putative replication licensing factor	1	9
TGGT1_227560	Putative IWS1 transcription factor	1	9
TGGT1_253940	CAM kinase family, incomplete catalytic triad	1	9
TGGT1_305510	Hypothetical protein	1	9
TGGT1_311625	WD domain, G-beta repeat-containing protein	1	9

unknown function 21 (DUF21) domain near the N terminus, followed by a CBS domain. Homology search in the human genome revealed that its homologs are cyclin M (CNNM) family proteins, which are plasma membrane metal transport mediator proteins involved in regulating intracellular Mg^{2+} homeostasis (41). Previous studies have shown that the CNNM family proteins are Mg^{2+} transporters that maintain intracellular Mg^{2+} levels by extruding Mg^{2+} from cells (41). Interestingly, PRLs were identified to interact with cyclin M (CNNM) family proteins physically, and the PRL-CNNM complex plays a significant role in regulating intracellular Mg^{2+} levels (42, 43). The identification of the *Toxoplasma* homolog by TgPRL co-IP indicates that the PRL-CNNM interaction is conserved in *Toxoplasma*.

Knockout of TgPRL increases intracellular Mg^{2+} levels. Studies in mammalian cells have shown that the CNNM family proteins maintain intracellular Mg^{2+} levels by extruding Mg^{2+} from cells (41). Through direct interaction with CNNMs, PRL regulates Mg^{2+} levels by inhibiting their Mg^{2+} efflux activity (42, 43). It has also been shown that PRL overexpression increases intracellular Mg^{2+} levels, and knockdown of PRL decreases Mg^{2+} levels (41). To explore if TgPRL plays a similar role in *Toxoplasma*, we compared intracellular Mg^{2+} levels among the parental, Δprl, and Δprl.cp strains by using the magnesium indicator Magnesium Green. Briefly, freshly lysed parasites from each of the three strains were incubated with Magnesium Green for 30 min before washes to remove extracellular Magnesium green. The washed parasites were resuspended with Magnesium Green-free medium and incubated for another 30 min to complete deesterification of intracellular AM esters. Parasites from the three strains were resuspended to the same concentration, and the same volume of parasites was added to a 96-well plate for fluorescence measurements. Surprisingly, the fluorescence signal of Δprl parasites was 38.2% $\pm$ 15.6% stronger than that of the parental strain, while that of the complemented strain was similar to that of the parental strain, suggesting that disruption of TgPRL increased intracellular Mg^{2+} levels, confirming a role for TgPRL in magnesium homeostasis (Fig. 5A). Moreover, we compared intracellular Mg^{2+} levels among the parental strain and the two mutant C339S and C401A complemented strains. Similarly, both mutant strains have significantly higher intracellular Mg^{2+} levels than the parental strain (Fig. 5B), indicating that the phosphatase activity of TgPRL is required for its function in regulating Mg^{2+} levels.

Parasites lacking TgPRL are avirulent to the mouse. We have found TgPRL is not essential but that its disruption affects parasite propagation in tissue culture, mainly due to a defect in host cell attachment. To explore if the tissue culture propagation
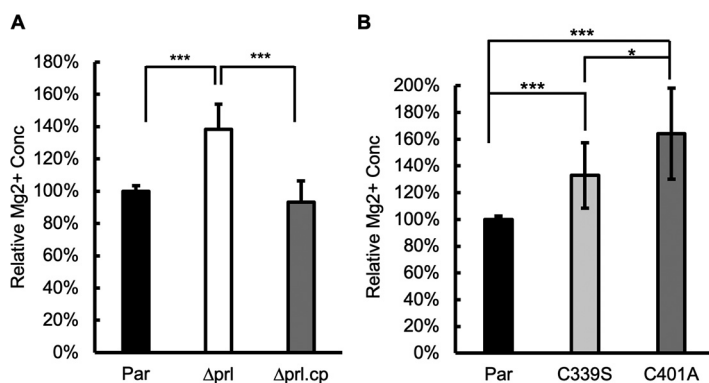
FIG 5 The TgPRL knockout parasite strain has a higher intracellular Mg^{2+} concentration. Bars show the relative intracellular free Mg^{2+} concentrations. (A) Comparison between the parental (Par), knockout (Δ*prl*), and complemented (Δ*prl*.cp) strains; (B) comparison between the parental strain and the two C339S and C401A mutant complemented strains. The data were from $n = 4$ biological replicates × 3 experimental replicates. For each biological replicate, data were normalized to the average of the parental. Error bars show standard deviations. *P* values are shown for comparisons between groups. ***, $P < 0.0001$; *, $P \leq 0.01$.

phenotype would manifest as an effect on parasite virulence *in vivo*, we injected CBA/J mice with either parental (Par), Δ*prl* (KO), or Δ*prl*.cp (Comp) parasites. Each parasite strain was injected into two groups of five mice, one with 100 parasites and the other with 10 parasites. An extra group of mice was injected with phosphate-buffered saline (PBS) as a control. As expected, all mice infected with the parental strain died, with those injected with 100 parasites succumbing by day 8 after injection and those injected with 10 by day 9 (Fig. 6). In each of the two groups of mice injected with Δ*prl*.cp parasites (Comp 100 and Comp 10), three mice died on day 9 (Fig. 6). Of the four remaining mice, three survived in good health, except one in the Comp 10 group, which died on day 20 (Fig. 6). Analysis of sera from the three surviving mice found no antibodies against parasites, suggesting that they were likely not infected (Fig. S2). Remarkably, all mice injected with the Δ*prl* parasites survived, whether they received 100 or 10 parasites (Fig. 6). All but one of the blood samples from the mice injected with the Δ*prl* parasites tested positive for anti-*Toxoplasma* antibodies (Fig. S2), indicating that the mice were efficiently infected but that the Δ*prl* strain is avirulent in mice.

To investigate if the antibodies produced by these surviving mice could confer protection against a subsequent *Toxoplasma* infection, we challenged all of the surviving mice with an injection of 100 parental parasites 2 weeks after blood collection. Unsurprisingly, all the antibody-negative mice died on day 8 after the challenge. Excitingly, all nine antibody-positive mice that had been infected with the Δ*prl* strain survived in good health (Fig. 6). Taken together, the findings of this *in vivo* experiment showed that disruption of TgPRL renders the parasite avirulent to mice and that infection with Δ*prl* parasites immunizes mice.

DISCUSSION

In the present study, we characterize the tyrosine phosphatase PRL in *Toxoplasma*. Similar to mammalian homologs, N-terminal epitope-tagged TgPRL localizes mainly to the plasma membrane, with some punctate localization in the cytoplasm. Mutation of the cysteine residue in the prenylation motif deprives TgPRL of plasma membrane localization, suggesting that prenylation is required to associate TgPRL with the plasma membrane. Knockout of *TgPRL* is not lethal to the parasites but affects their growth in tissue culture, primarily due to a defect in host cell attachment. The link between TgPRL and host cell attachment adds new insights to our understanding of attachment, one of the key lytic cycle steps of *Toxoplasma* (8). For intracellular parasites, efficient entry of host cells is essential to parasitize a wide range of host cells. *Toxoplasma* can parasitize almost any warm-blooded animal because of its unique gift to attach to
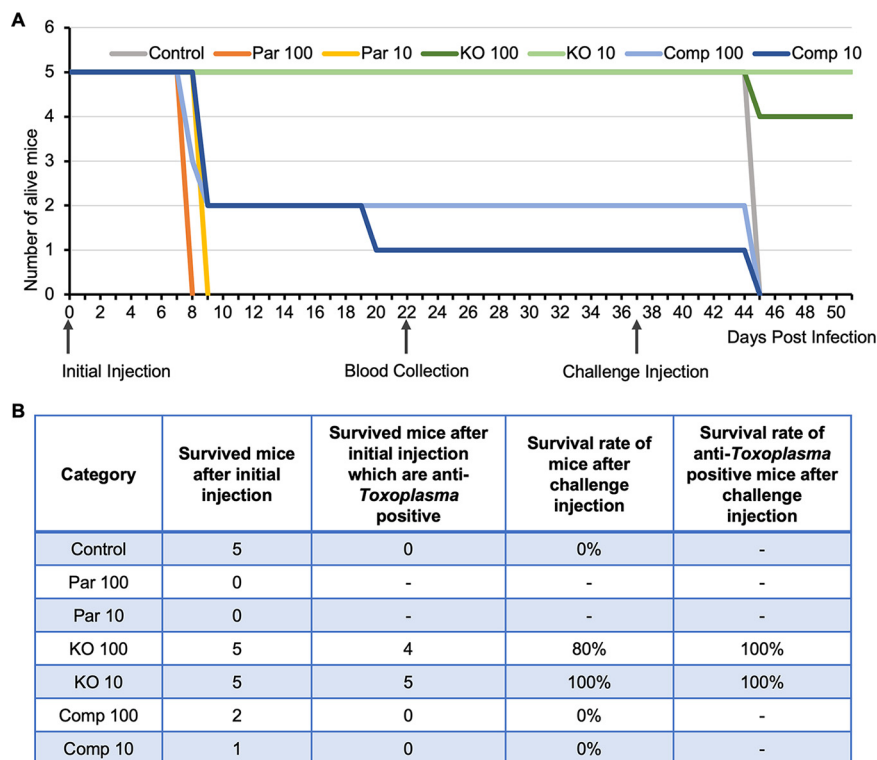
FIG 6 The TgPRL knockout strain is avirulent in mice. Mice were separated into groups, and each mouse was injected with either 10 or 100 parasites of the parental (Par 10 and 100), knockout (KO 10 and 100), and complemented (Comp 10 and 100) strains. (A) Animals were monitored after infection, and the day of death was recorded. The graph shows the survival curves of the mice for each of the infected groups. The three arrows pointing at the *x* axis indicate the days of the initial injection, blood collection, and challenge injection, respectively. (B) The table shows the number of mice that survived in each test group after the initial injection, the number of mice that tested positive for anti-*Toxoplasma* antibodies, and the survival rate of anti-*Toxoplasma* antibody-positive mice after challenge injection.

and invade host cells. For *Toxoplasma*, adhesion proteins secreted from micronemes help the parasite establish a tight interaction with the host cell (38, 44), and the glideo-some-centered motility system provides a strong impetus for entering the host cell (45). Recent studies have recognized that *Toxoplasma* attachment to host cells appears to be regulated by more than just microneme secretion. In our previous study, we found that PPM5C, a protein phosphatase of the PP2C family, plays an important role in attachment to host cells that is unrelated to microneme secretion (22). In addition, calcineurin, a PPP family protein phosphatase, is necessary for both *Toxoplasma* and *Plasmodium falciparum* to strongly attach to host cells before entry, which is also not related to microneme secretion (46). In this study, we have determined that the tyrosine phosphatase TgPRL is required for efficient host cell attachment in *Toxoplasma*. Complete knockout of TgPRL reduces the parasite's ability to attach firmly to the host cell by almost 80%. However, knockout of TgPRL did not seem to affect microneme secretion. While this result suggests TgPRL's role in attachment is independent of microneme secretion in general, it is plausible that TgPRL directly or indirectly regulates specific proteins involved in the process. Similarly, other aspects of the parasite's biology, such as shape, membrane rigidity, and osmotic pressure, could influence attachment and be the target of TgPRL regulation.

Interestingly, we have determined that the disruption of TgPRL increases intracellular free Mg^{2+} concentration in *Toxoplasma*. A role for PRL phosphatases in regulating magnesium homeostasis has been reported in mammalian cells (43). This function appears to be driven by a direct interaction between PRL and cyclin M (CNNM) family proteins (42, 47). CNNM family proteins contain two evolutionarily conserved domains,

with a transmembrane unknown function 21 (DUF21) domain at the N terminus, which spans the plasma membrane, followed by a cystathionine-β-synthase (CBS) domain (41). Previous studies have shown that the CNNM family proteins are Mg^{2+} transporters that maintain intracellular Mg^{2+} levels by extruding Mg^{2+} from the cell and that the formation of PRL-CNNM complex inhibits Mg^{2+} efflux (41). This interaction is dependent on a conserved aspartic acid residue in the CBS domain of CNNM, and mutation of this key amino acid blocks the PRL-CNNM interaction and results in the release of inhibition of Mg^{2+} efflux (43). Moreover, PRL-CNNM interaction seems to be regulated by the phosphorylation status of the cysteine in the center of the phosphatase domain of PRL (43). This showed that phosphorylation of this cysteine blocks the interaction and that phospho-cysteine levels change in response to intracellular Mg^{2+} levels (43).

Toxoplasma encodes two proteins with both DUF21 and CBS domains (TGGT1_211350 and TGGT1_307580). Of these two, TGGT1_211350 is most similar to mammalian homologs—hence the name CNNM1. Interestingly, unbiased identification of proteins that interact with TgPRL revealed CNNM1 as one of the top hit proteins, suggesting the PRL-CNNM complex is also present in *Toxoplasma*. If present, this complex may also regulate intracellular Mg^{2+} homeostasis in the plasma membrane, as it does in mammalian cells. Unfortunately, various attempts to add an epitope tag to the C terminus of endogenous CNNM1 or to express exogenous CNNM1 with an epitope tag at the N terminus or between the DUF21 and CBS domains failed, which hindered our efforts to study this interaction in *Toxoplasma* further. Nonetheless, our observation that Mg^{2+} levels are disrupted in the TgPRL mutant strongly suggests that the interaction between TgPRL and CNNM1 is present in the parasite. Interestingly, disruption of TgPRL resulted in an increase in intracellular free Mg^{2+} rather than the decrease in intracellular Mg^{2+} levels seen when the mammalian homolog is disrupted (41). Thus, it appears that there might be a different function for the PRL-CNNM interaction in *Toxoplasma*. In fact, the similarity between TgCNNM1 and mammalian homologs is only present in the DUF21 and CBS domains, a small portion of TgCNNM1 located in the N-terminal region. The majority of TgCNNM1 does not show any homology with mammalian homologs, and TgCNNM1 is approximately 2 times the size of mammalian homologs. Additionally, because *Toxoplasma* resides in the host cell, its extracellular environment is also different from that of mammalian cells. Therefore, it would not be surprising if the PRL-CNNM complex does not have the same functional properties as the mammalian counterpart. How the dysregulation of Mg^{2+} homeostasis in the TgPRL mutant connects to the defect in attachment is unclear. Plausibly, an increase of intracellular Mg^{2+} concentration in the Δprl parasite may trigger some effects, such as it may alter the osmotic pressure of the parasite or possibly allow parasites to maintain a higher level of $ATP-Mg^{2+}$, while parasites with an additional energy supply may be more inclined to remain free or may overactivate enzymes, leading to complex physiological changes or triggering disturbances in the metabolism of other ions in the cell.

The co-IP of TgPRL identified other potential interacting proteins with variable functions, suggesting the involvement of TgPRL in multiple pathways. The top two hits of the co-IP are two unknown FHA domain-containing proteins (TGGT1_287980 and TGGT1_202840), both of which probably play key roles based on their low fitness scores (-3.15 and -3.54) (36). Notably, three proteins in this list are potentially associated with endocytosis in *Toxoplasma* (48). They are TgK13 (TGGT1_262150), the homolog of *Plasmodium* Kelch13 (K13), TgEps15 (TGGT1_227800), and TgPPG1 (TGGT1_297520). A previous study reported that K13 plays an important role in *Plasmodium* endocytosis and that Eps15 and PPG1 are two partners of K13 that colocalize with K13 in the hemoglobin-containing endocytic compartment in *Plasmodium* (49). Although little is known about endocytosis in *Toxoplasma*, a large number of proteins required for endocytosis are encoded in its genome, including the three shown here (48). The IFA of N-terminal HA-tagged TgPRL showed that in addition to being localized to the plasma membrane, TgPRL is also present in the cytoplasm in a punctate form. Therefore, those puncta with TgPRL localization may be endocytic compartments in *Toxoplasma*.

One of the most significant findings of our characterization of TgPRL is the discovery that this protein is an essential virulence factor. Mice infected with as many as 100 Δ*prl* parasites survive infection and mount immunity against challenges with parental parasites. This avirulent phenotype is remarkable as the parental strain is highly virulent, with one parasite killing mice within 10 days (50), and the mutant can propagate effectively in tissue culture, albeit more slowly than the parental strain. This result underscores the critical role of TgPRL in the biology of *Toxoplasma* and reveals this protein as a strong candidate for therapeutic intervention. Future studies on the molecular mechanisms underlying TgPRL function will reveal important information about *Toxoplasma*'s virulence and propagation in infected tissues.

MATERIALS AND METHODS

Parasite cultures. All parasites were cultured and maintained in human foreskin fibroblasts (HFFs) as previously described (22). The growth medium used was Dulbecco's modified Eagle's medium (DMEM) supplemented with 10% fetal bovine serum (FBS), 2 mM L-glutamine, and 50 μg/mL penicillin-streptomycin. The parasites used in this study include strain RH lacking hypoxanthine-xanthine-guanine phosphoribosyl transferase (HXGPRT) (RH Δ*hxgprt* [referred to here as Δ*hx*]) (51) and RH lacking HXGPRT and Ku80 (RH Δ*ku80* Δ*hxgprt* [referred to here as Δ*ku80*]) (35). To harvest intracellular parasites, infected cells were scraped off and passed through a 27-gauge needle.

Generation of HA-PRL expression parasite line. For cloning experiments, genomic DNA was isolated from Δ*ku80* parasites, and cDNA was prepared from total RNA isolated from Δ*ku80* parasites as described before (22). To generate the plasmid for exogenous expression of HA-PRL, the TgPRL coding region was amplified by PCR from cDNA using a forward primer that encodes a hemagglutinin (HA) epitope tag coding sequence in frame with *TgPRL*. All primers used in this study are included in Table S1 in the supplemental material. To drive expression of the exogenous TgPRL, we amplified an ~800-bp genomic DNA region immediately preceding the start codon of the *TgPRL* gene to include the *TgPRL* promoter and 5' UTR (PRL.pr). The PRL.pr and HA-PRL amplicons were cloned into a plasmid backbone containing a tubulin 3' UTR and an HXGPRT selection cassette using In-Fusion HD cloning to obtain the plasmid pPRL.pr-HA-PRL-Tub-HXGPRT. This plasmid was linearized and transfected into the Δ*hx* *Toxoplasma* strain by electroporation. Stably transfected parasites were selected for in 50 mg/mL mycophenolic acid (MPA), and 50 mg/mL xanthine, and clones were established by limiting dilution.

Generation of TgPRL knockout strain. The CRISPR/Cas9 plasmid pSag1-Cas9-U6-sgPRL-HXG was generated by mutating the single guide RNA (sgRNA) in the pSag1-Cas9-U6-sgUPRT-HXG plasmid (33) (a gift from David Sibley) into the sgRNA targeting the first exon of the *TgPRL* gene by using the Q5 site-directed mutagenesis kit (NEB). A DNA fragment containing the DHFR selection cassette flanked by short homology to upstream and downstream of the guide RNA target site was amplified using pJET-DHFR (a gift from Peter Bradley) as a template. The pSag1-Cas9-U6-sgPRL-HXG plasmid and the PCR amplicon were transfected together into Δ*ku80* parasites. The transfected parasites were treated with 1 mM pyrimethamine for selection, and the parasites were cloned by limiting dilution. Clones were tested by PCR, and the resulting amplicons were sequenced to confirm the expected disruption of *TgPRL*.

Complementation with TgPRL WT and mutated cDNA. The complementation with wild type (WT) TgPRL used the same plasmid, pPRL.pr-HA-PRL-Tub-HXGPRT, used for generation of the HA-PRL expression line. The complementation constructs with mutant TgPRL were generated by introducing synthesized DNA fragments with either the C339S or C401A mutations by In-Fusion HD cloning into the complementing plasmid digested with NotI and NcoI or NcoI and AflII. The resulting plasmids were named pPRL.pr-HA-PRL.C339S-Tub-HXGPRT and pPRL.pr-HA-PRL.C401A-Tub-HXGPRT.

The TgPRL WT and mutant complementation plasmids were used as the templates to amplify the PRL.pr-HA-PRL-Tub expression cassette plus the HXGPRT selection maker cassette for complementation. To direct the resulting amplicon to insert into the 5' UTR of the disrupted KU80 gene in the Δ*prl* parasite strain, a CRISPR/Cas9 plasmid pSag1-Cas9-U6-sgKU80.5'UTR-HXG was generated by mutating the sgRNA in the pSag1-Cas9-U6-sgUPRT-HXG plasmid into the sgRNA targeting the 5' UTR of the KU80 gene by using the Q5 site-directed mutagenesis kit. Both the amplicon and pSag1-Cas9-U6-sgKU80.5'UTR-HXG plasmid were transfected into Δ*prl* parasite strain. The transfected parasites were selected with 50 mg/mL MPA and 50 mg/mL xanthine in culture and then cloned by limiting dilution.

Immunofluorescence assays and Western blots. Both immunofluorescence assays (IFAs) and Western blots were performed with previously described protocols (22). For this study, the primary antibodies used were rabbit anti-HA (Cell Signaling Technology) and rat anti-IMC3, both used at 1:1,000. For the IFA, the secondary antibodies were Alexa Fluor 594- or Alexa Fluor 488-conjugated goat anti-rabbit and goat anti-rat (Invitrogen), both used at 1:2,000. Imaging was performed with a Nikon Eclipse E100080i microscope at ×100 magnification. For Western blots, we used anti-rabbit or anti-mouse secondary antibodies conjugated to horseradish peroxidase (HRP)-labeled IgG.

Phenotypic assays. All of the phenotypic assays were performed with standard methods previously described (52). Briefly, for plaque assays, each well of a 12-well plate with confluent HFF monolayers was infected with 500 freshly syringe-released parasites. Cultures were allowed to be incubated for 6 days before being fixed with methanol and stained with crystal violet. Imaging was performed using a ProteinSimple imaging system, and the relative plaque areas were measured by ImageJ and the plugin ColonyArea (53). For doubling assays, 2×10^4 freshly syringe-released parasites were allowed to invade

HFFs for 30 min. Cultures were washed with DMEM four times to remove free parasites and then incubated for 18, 24, and 30 h before being fixed with methanol and stained with the Hema3 manual staining system (Fisher Scientific). For each sample, 50 vacuoles were randomly selected, and the number of parasites per vacuole was recorded and converted to corresponding rounds of division.

To perform vacuole formation assays, 5×10^5 freshly syringe-released and filter-purified parasites were allowed to invade HFFs for 30 min. Unstably attached and unattached parasites were removed by four washes with DMEM, and the cultures were incubated for about 24 h before fixation with methanol and staining with the Hema3 manual staining system. For each sample, 10 fields of views were randomly selected and scored for the number of vacuoles.

For red/green invasion assays, coverslips with HFF monolayers were infected with 1 mL of parasites at a concentration of 2.5×10^6 parasites/mL for 30 min and then were washed with DMEM three times and fixed with 4% methanol-free paraformaldehyde for 15 min. After being quenched with 0.1 M glycine and washed with PBS three times, the samples were incubated with mouse anti-Sag1 (1:2,000) antibody in 3% bovine serum albumin (BSA)–PBS for 40 min, followed by three washes with PBS. The samples were then permeabilized and treated as described above for IFAs using rabbit anti-Mic5 (1:2,000) as the primary antibody and goat anti-rabbit/mouse conjugated with Alexa Fluor 594/488 (1:2,000) as the secondary antibody. For each coverslip, 10 views were randomly selected for counting extracellular (attached but not invaded [green]) and total (both extracellular and intracellular [red]) parasites.

Microneme secretion assay. As described before (22), freshly lysed parasites were harvested and resuspended with invasion medium (DMEM, 1.5 g/L NaHCO₃, 20 mM HEPES [pH 7.4], and 3% FBS) at a concentration of 1×10^9 parasites/mL. Two aliquots of 100 μL of the parasite suspension were used for each sample: one for ethanol-stimulated secretion and the other for natural secretion. For ethanol-stimulated secretion, 2% ethanol was added to each sample. Ethanol-treated samples were incubated at 37°C for 10 min, and natural secretion samples were incubated at 37°C for 1 h. After incubation, the samples were centrifuged at $1,000 \times g$ for 3 min, 80 μL of supernatant was collected and subjected to a second centrifugation, and finally, 60 μL of the new supernatant was used for Western blotting. The pellets from the first centrifugation were resuspended with PBS and centrifuged again, the final pellets were lysed with radioimmunoprecipitation assay (RIPA) buffer, and the lysates were used for Western blotting.

Cross-linking and immunoprecipitation. As described previously (22), freshly lysed parasites were harvested and incubated for 10 min in PBS with 5 mM DSSO. Tris buffer was added to a final concentration of 20 mM to quench the reaction at room temperature for 5 min. After washes, the parasites were lysed with 1 mL RIPA lysis buffer containing a protease and phosphatase inhibitor cocktail at 4°C for 1 h. The lysate was then centrifuged, and the supernatant was incubated with 25 μL of mouse IgG magnetic beads (Cell Signaling) for 1 h at room temperature for precleaning. The unbound lysate was separated from the IgG beads and was incubated with 25 μL of anti-HA magnetic beads (Fisher Scientific) for another hour at room temperature. The anti-HA magnetic beads were washed with RIPA lysis buffer and PBS and then submitted to the Indiana University School of Medicine Proteomics Core facility for mass spectrometry.

Intracellular magnesium concentration measurements. Freshly lysed parasites were harvested and centrifuged at $1,000 \times g$ for 10 min. The parasites were resuspended with 1 mL of prewarmed buffer A (116 mM NaCl, 5.4 mM KCl, 0.8 mM MgSO₄, 5.5 mM D-glucose, and 50 mM HEPES [pH 7.4]) with 5 mM Magnesium Green (Invitrogen) and incubated at 37°C for 30 min. After incubation, the parasites were washed with buffer A two times to remove extracellular Magnesium Green and then resuspended with buffer A at a concentration of 3×10^7 parasites/mL and incubated at 37°C for another 30 min to allow the complete deesterification of intracellular AM esters. After incubation, 100 μL of parasites was loaded into each well of a 96-well black/clear-bottom plate. A Synergy Plate Reader was used to measure fluorescence with excitation at 488 nm and emission at 531 nm.

Mouse injection and blood collection and serum antibody detection. All experiments using mice were performed with the approval of the Institutional Animal Care and Use Committee (IACUC) of Indiana University School of Medicine (IUSM) and in strict compliance with the National Institutes of Health (NIH) *Guide for the Care and Use of Laboratory Animals* (54). The 35 mice used in this study were female CBA/J mice aged 6 to 8 weeks, and they were divided into seven groups with five mice in each. Parasites for injection were syringe released from infected cells and resuspended in PBS to a concentration of 1,000 parasites/mL or 100 parasites/mL. One hundred microliters of PBS with 100 or 10 parasites of each strain was injected into each mouse intraperitoneally. The control group of mice was injected with 100 μL of 1$\times$ PBS.

Blood samples from surviving mice were collected from the submandibular vein. Mouse sera were used in immunoblotting assays to detect anti-*Toxoplasma* antibodies. Briefly, 5 μL of 1$\times$ PBS containing 10^5 freshly lysed *Toxoplasma* parasites were blotted onto a piece of nitrocellulose membrane and allowed to dry. The membranes were placed into 24-well plates, blocked with 5% nonfat dry milk (NFDM)–Tris-buffered saline plus Tween 20 (TBST) for 45 min, and then incubated with 1:50-diluted sera isolated from the blood samples in 5% NFDM–TBST for 1 h. After three washes with TBST, the membranes were incubated with horseradish peroxidase-conjugated anti-mouse IgG in 5% NFDM–TBST for 1 h. After three washes with TBST, the membranes were treated with SuperSignal West Pico chemiluminescent substrate (Pierce Chemical) and imaged using FluorChem E (ProteinSimple).

SUPPLEMENTAL MATERIAL

Supplemental material is available online only.

FIG S1, PDF file, 0.03 MB.

FIG S2, PDF file, 0.05 MB.

TABLE S1, PDF file, 0.03 MB.
DATA SET S1, PDF file, 0.1 MB.

REFERENCES

1. Hill DE, Chirukandoth S, Dubey JP. 2005. Biology and epidemiology of Toxoplasma gondii in man and animals. Anim Health Res Rev 6:41–61. https://doi.org/10.1079/ahr2005100.
2. Pappas G, Roussos N, Falagas ME. 2009. Toxoplasmosis snapshots: global status of Toxoplasma gondii seroprevalence and implications for pregnancy and congenital toxoplasmosis. Int J Parasitol 39:1385–1394. https://doi.org/10.1016/j.ijpara.2009.04.003.
3. Dubey JP, Lindsay DS, Speer CA. 1998. Structures of Toxoplasma gondii tachyzoites, bradyzoites, and sporozoites and biology and development of tissue cysts. Clin Microbiol Rev 11:267–299. https://doi.org/10.1128/CMR.11.2.267.
4. Porter SB, Sande MA. 1992. Toxoplasmosis of the central nervous system in the acquired immunodeficiency syndrome. N Engl J Med 327:1643–1648. https://doi.org/10.1056/NEJM199212033272306.
5. Wong SY, Remington JS. 1994. Toxoplasmosis in pregnancy. Clin Infect Dis 18:853–861. https://doi.org/10.1093/clinids/18.6.853.
6. Khan K, Khan W. 2018. Congenital toxoplasmosis: an overview of the neurological and ocular manifestations. Parasitol Int 67:715–721. https://doi.org/10.1016/j.parint.2018.07.004.
7. Black MW, Boothroyd JC. 2000. Lytic cycle of Toxoplasma gondii. Microbiol Mol Biol Rev 64:607–623. https://doi.org/10.1128/MMBR.64.3.607-623.2000.
8. Blader IJ, Coleman BI, Chen CT, Gubbels MJ. 2015. Lytic cycle of Toxoplasma gondii: 15 years later. Annu Rev Microbiol 69:463–485. https://doi.org/10.1146/annurev-micro-091014-104100.
9. Carruthers VB, Giddings OK, Sibley LD. 1999. Secretion of micronemal proteins is associated with toxoplasma invasion of host cells. Cell Microbiol 1:225–235. https://doi.org/10.1046/j.1462-5822.1999.00023.x.
10. Hakansson S, Morisaki H, Heuser J, Sibley LD. 1999. Time-lapse video microscopy of gliding motility in Toxoplasma gondii reveals a novel, biphasic mechanism of cell locomotion. Mol Biol Cell 10:3539–3547. https://doi.org/10.1091/mbc.10.11.3539.
11. Jia Y, Marq JB, Bisio H, Jacot D, Mueller C, Yu L, Choudhary J, Brochet M, Soldati-Favre D. 2017. Crosstalk between PKA and PKG controls pH-dependent host cell egress of Toxoplasma gondii. EMBO J 36:3250–3267. https://doi.org/10.15252/embj.201796794.
12. Brown KM, Sibley LD. 2018. Essential cGMP signaling in Toxoplasma is initiated by a hybrid P-type ATPase-guanylate cyclase. Cell Host Microbe 24:804–816.e6. https://doi.org/10.1016/j.chom.2018.10.015.
13. Uboldi AD, Wilde ML, McRae EA, Stewart RJ, Dagley LF, Yang L, Katris NJ, Hapuarachchi SV, Coffey MJ, Lehane AM, Botte CY, Waller RF, Webb AI, McConville MJ, Tonkin CJ. 2018. Protein kinase A negatively regulates Ca2+ signalling in Toxoplasma gondii. PLoS Biol 16:e2005642. https://doi.org/10.1371/journal.pbio.2005642.
14. Katris NJ, Ke H, McFadden GI, van Dooren GG, Waller RF. 2019. Calcium negatively regulates secretion from dense granules in Toxoplasma gondii. Cell Microbiol 21:e13011. https://doi.org/10.1111/cmi.13011.
15. Gaji RY, Johnson DE, Treeck M, Wang M, Hudmon A, Arrizabalaga G. 2015. Phosphorylation of a myosin motor by TgCDPK3 facilitates rapid initiation of motility during Toxoplasma gondii egress. PLoS Pathog 11:e1005268. https://doi.org/10.1371/journal.ppat.1005268.
16. Hortua Triana MA, Marquez-Nogueras KM, Vella SA, Moreno SNJ. 2018. Calcium signaling and the lytic cycle of the apicomplexan parasite Toxoplasma gondii. Biochim Biophys Acta Mol Cell Res 1865:1846–1856. https://doi.org/10.1016/j.bbamcr.2018.08.004.
17. Tang Q, Andenmatten N, Hortua Triana MA, Deng B, Meissner M, Moreno SN, Ballif BA, Ward GE. 2014. Calcium-dependent phosphorylation alters class XIVa myosin function in the protozoan parasite Toxoplasma gondii. Mol Biol Cell 25:2579–2591. https://doi.org/10.1091/mbc.E13-11-0648.
18. Bansal P, Antil N, Kumar M, Yamaryo-Botte Y, Rawat RS, Pinto S, Datta KK, Katris NJ, Botte CY, Prasad TSK, Sharma P. 2021. Protein kinase TgCDPK7 regulates vesicular trafficking and phospholipid synthesis in Toxoplasma gondii. PLoS Pathog 17:e1009325. https://doi.org/10.1371/journal.ppat.1009325.
19. Garrison E, Treeck M, Ehret E, Butz H, Garbuz T, Oswald BP, Settles M, Boothroyd J, Arrizabalaga G. 2012. A forward genetic screen reveals that calcium-dependent protein kinase 3 regulates egress in Toxoplasma. PLoS Pathog 8:e1003049. https://doi.org/10.1371/journal.ppat.1003049.
20. Varberg JM, Coppens I, Arrizabalaga G, Gaji RY. 2018. TgTKL1 is a unique plant-like nuclear kinase that plays an essential role in acute toxoplasmosis. mBio 9:e00301-18. https://doi.org/10.1128/mBio.00301-18.
21. McCoy JM, Whitehead L, van Dooren GG, Tonkin CJ. 2012. TgCDPK3 regulates calcium-dependent egress of Toxoplasma gondii from host cells. PLoS Pathog 8:e1003066. https://doi.org/10.1371/journal.ppat.1003066.
22. Yang C, Broncel M, Dominicus C, Sampson E, Blakely WJ, Treeck M, Arrizabalaga G. 2019. A plasma membrane localized protein phosphatase in Toxoplasma gondii, PPM5C, regulates attachment to host cells. Sci Rep 9:5924. https://doi.org/10.1038/s41598-019-42441-1.
23. Hardy S, Kostantin E, Hatzihristidis T, Zolotarov Y, Uetani N, Tremblay ML. 2018. Physiological and oncogenic roles of the PRL phosphatases. FEBS J 285:3886–3908. https://doi.org/10.1111/febs.14503.
24. Diamond RH, Cressman DE, Laz TM, Abrams CS, Taub R. 1994. PRL-1, a unique nuclear protein tyrosine phosphatase, affects cell growth. Mol Cell Biol 14:3752–3762. https://doi.org/10.1128/mcb.14.6.3752-3762.1994.
25. Zeng Q, Si X, Horstmann H, Xu Y, Hong W, Pallen CJ. 2000. Prenylation-dependent association of protein-tyrosine phosphatases PRL-1, -2, and -3 with the plasma membrane and the early endosome. J Biol Chem 275:21444–21452. https://doi.org/10.1074/jbc.M000453200.
26. Wang J, Kirby CE, Herbst R. 2002. The tyrosine phosphatase PRL-1 localizes to the endoplasmic reticulum and the mitotic spindle and is required for normal mitosis. J Biol Chem 277:46659–46668. https://doi.org/10.1074/jbc.M206407200.
27. Li J, Guo K, Koh VWC, Tang JP, Gan BQ, Shi H, Li HX, Zeng Q. 2005. Generation of PRL-3 and PRL-1 specific monoclonal antibodies as potential diagnostic markers for cancer metastases. Clin Cancer Res 11:2195–2204. https://doi.org/10.1158/1078-0432.CCR-04-1984.
28. Duciel L, Monraz Gomez LC, Kondratova M, Kuperstein I, Saule S. 2019. The phosphatase PRL-3 is involved in key steps of cancer metastasis. J Mol Biol 431:3056–3067. https://doi.org/10.1016/j.jmb.2019.06.008.
29. Rubio T, Kohn M. 2016. Regulatory mechanisms of phosphatase of regenerating liver (PRL)-3. Biochem Soc Trans 44:1305–1312. https://doi.org/10.1042/BST20160146.
30. Guzińska-Ustymowicz K, Pryczynicz A. 2011. PRL-3, an emerging marker of carcinogenesis, is strongly associated with poor prognosis. Anticancer Agents Med Chem 11:99–108. https://doi.org/10.2174/187152011794941145.
31. Wei M, Korotkov KV, Blackburn JS. 2018. Targeting phosphatases of regenerating liver (PRLs) in cancer. Pharmacol Ther 190:128–138. https://doi.org/10.1016/j.pharmthera.2018.05.014.
32. Pendyala PR, Ayong L, Eatrides J, Schreiber M, Pham C, Chakrabarti R, Fidock DA, Allen CM, Chakrabarti D. 2008. Characterization of a PRL protein tyrosine phosphatase from Plasmodium falciparum. Mol Biochem Parasitol 158:1–10. https://doi.org/10.1016/j.molbiopara.2007.11.006.
33. Shen B, Brown K, Long S, Sibley LD. 2017. Development of CRISPR/Cas9 for efficient genome editing in Toxoplasma gondii. Methods Mol Biol 1498:79–103. https://doi.org/10.1007/978-1-4939-6472-7_6.

34. Donald RG, Roos DS. 1993. Stable molecular transformation of Toxoplasma gondii: a selectable dihydrofolate reductase-thymidylate synthase marker based on drug-resistance mutations in malaria. Proc Natl Acad Sci U S A 90:11703–11707. https://doi.org/10.1073/pnas.90.24.11703.

35. Huynh MH, Carruthers VB. 2009. Tagging of endogenous genes in a Toxoplasma gondii strain lacking Ku80. Eukaryot Cell 8:530–539. https://doi.org/10.1128/EC.00358-08.

36. Sidik SM, Huet D, Ganesan SM, Huynh MH, Wang T, Nasamu AS, Thiru P, Saeij JPJ, Carruthers VB, Niles JC, Lourido S. 2016. A genome-wide CRISPR screen in Toxoplasma identifies essential apicomplexan genes. Cell 166:1423–1435.e12. https://doi.org/10.1016/j.cell.2016.08.019.

37. Huynh MH, Rabenau KE, Harper JM, Beatty WL, Sibley LD, Carruthers VB. 2003. Rapid invasion of host cells by Toxoplasma requires secretion of the MIC2-M2AP adhesive protein complex. EMBO J 22:2082–2090. https://doi.org/10.1093/emboj/cdg217.

38. Carruthers VB, Tomley FM. 2008. Microneme proteins in apicomplexans. Subcell Biochem 47:33–45. https://doi.org/10.1007/978-0-387-78267-6_2.

39. Wetzel DM, Chen LA, Ruiz FA, Moreno SN, Sibley LD. 2004. Calcium-mediated protein secretion potentiates motility in Toxoplasma gondii. J Cell Sci 117:5739–5748. https://doi.org/10.1242/jcs.01495.

40. Guan KL, Dixon JE. 1991. Evidence for protein-tyrosine-phosphatase catalysis proceeding via a cysteine-phosphate intermediate. J Biol Chem 266:17026–17030. https://doi.org/10.1016/S0021-9258(19)47335-3.

41. Funato Y, Miki H. 2019. Molecular function and biological importance of CNNM family Mg2+ transporters. J Biochem 165:219–225. https://doi.org/10.1093/jb/mvy095.

42. Hardy S, Uetani N, Wong N, Kostantin E, Labbe DP, Begin LR, Mes-Masson A, Miranda-Saavedra D, Tremblay ML. 2015. The protein tyrosine phosphatase PRL-2 interacts with the magnesium transporter CNNM3 to promote oncogenesis. Oncogene 34:986–995. https://doi.org/10.1038/onc.2014.33.

43. Gulerez I, Funato Y, Wu H, Yang M, Kozlov G, Miki H, Gehring K. 2016. Phosphocysteine in the PRL-CNNM pathway mediates magnesium homeostasis. EMBO Rep 17:1890–1900. https://doi.org/10.15252/embr.201643393.

44. Liu Q, Li FC, Zhou CX, Zhu XQ. 2017. Research advances in interactions related to Toxoplasma gondii microneme proteins. Exp Parasitol 176:89–98. https://doi.org/10.1016/j.exppara.2017.03.001.

45. Opitz C, Soldati D. 2002. The 'glideosome': a dynamic complex powering gliding motion and host cell invasion by Toxoplasma gondii. Mol Microbiol 45:597–604. https://doi.org/10.1046/j.1365-2958.2002.03056.x.

46. Paul AS, Saha S, Engelberg K, Jiang RH, Coleman BI, Kosber AL, Chen CT, Ganter M, Espy N, Gilberger TW, Gubbels MJ, Duraisingh MT. 2015. Parasite calcineurin regulates host cell recognition and attachment by apicomplexans. Cell Host Microbe 18:49–60. https://doi.org/10.1016/j.chom.2015.06.003.

47. Funato Y, Yamazaki D, Mizukami S, Du L, Kikuchi K, Miki H. 2014. Membrane protein CNNM4-dependent Mg2+ efflux suppresses tumor progression. J Clin Invest 124:5398–5410. https://doi.org/10.1172/JCI76614.

48. McGovern OL, Rivera-Cuevas Y, Carruthers VB. 2021. Emerging mechanisms of endocytosis in Toxoplasma gondii. Life (Basel) 11:84. https://doi.org/10.3390/life11020084.

49. Birnbaum J, Scharf S, Schmidt S, Jonscher E, Hoeijmakers WAM, Flemming S, Toenhake CG, Schmitt M, Sabitzki R, Bergmann B, Frohlke U, Mesen-Ramirez P, Blancke Soares A, Herrmann H, Bartfai R, Spielmann T. 2020. A Kelch13-defined endocytosis pathway mediates artemisinin resistance in malaria parasites. Science 367:51–59. https://doi.org/10.1126/science.aax4735.

50. Sibley LD, Boothroyd JC. 1992. Virulent strains of Toxoplasma gondii comprise a single clonal lineage. Nature 359:82–85. https://doi.org/10.1038/359082a0.

51. Donald RG, Carter D, Ullman B, Roos DS. 1996. Insertional tagging, cloning, and expression of the Toxoplasma gondii hypoxanthine-xanthine-guanine phosphoribosyltransferase gene. Use as a selectable marker for stable transformation. J Biol Chem 271:14010–14019. https://doi.org/10.1074/jbc.271.24.14010.

52. LaFavers KA, Marquez-Nogueras KM, Coppens I, Moreno SNJ, Arrizabalaga G. 2017. A novel dense granule protein, GRA41, regulates timing of egress and calcium sensitivity in Toxoplasma gondii. Cell Microbiol 19:10.1111/cmi.12749. https://doi.org/10.1111/cmi.12749.

53. Guzman C, Bagga M, Kaur A, Westermarck J, Abankwa D. 2014. ColonyArea: an ImageJ plugin to automatically quantify colony formation in clonogenic assays. PLoS One 9:e92444. https://doi.org/10.1371/journal.pone.0092444.

54. National Research Council. 2011. Guide for the care and use of laboratory animals, 8th ed. National Academies Press, Washington, DC.